Microscopic structure of a pure near-critical fluid confined to a mesoscopic slit-pore

Martin Schoen*
Institut für Theoretische Physik, Technische Universität Berlin, Hardenbergstrasse 36, 10623 Berlin, Germany

Matthias Thommes
I.-N.-Stranski-Institut für Physikalische und Theoretische Chemie, Technische Universität Berlin, Straße-des-17.-Juni 112, 10623 Berlin, Germany

(Received 30 May 1995)

The adsorption behavior of a near-critical fluid (pore fluid) in a mesoscopic slit-pore is investigated in grand canonical ensemble Monte Carlo (GCEMC) simulations. In these simulations the chemical potential $\mu(T)$ (T is the temperature) is chosen such that the pore fluid is in thermodynamic equilibrium with a homogeneous bulk fluid reservoir maintained at the critical density ρ_c. These conditions mimic recent adsorption experiments [M. Thommes, G. H. Findenegg, and H. Lewandowski, Ber. Bunsenges. Phys. Chem. **98**, 477 (1994)] in which, after a maximum, a sharp decrease of the pore *average* density ρ_p is observed as T approaches T_c from above (i.e., $T \to T_c +$). The GCEMC simulations offer a microscopic explanation of this effect in terms of the local density $\rho^{(1)}(z)$ of the pore fluid. It is found that the mean density in the core region of the pore and the mean density of the first layers next to the walls exhibit an opposite temperature dependence: while the density near the wall increases with decreasing temperature (as is to be expected for sufficiently strong attractive fluid-wall interactions) the density in the core region decreases and falls below ρ_c as $T \to T_c +$. This latter effect dominates in the near-critical region and causes a net decrease of the pore density. This depletion effect is different from drying which is characterized by a decreasing density in the vicinity of the walls. Depletion depends on the interplay between the strength of the fluid-wall potential and the width of the pore's cross section. By employing a two-fluid van der Waals model for the fluid in the core region and the bulk reservoir it is shown that depletion is closely related to restricted density fluctuations in confined fluids.

PACS number(s): 05.70.Jk, 61.20.Ja, 68.15.+e, 68.35.Rh

I. INTRODUCTION

In the vicinity of the critical point (i.e., in the *near-critical regime)* many properties of a fluid change dramatically. At the molecular level this may often be ascribed to a power-law divergence of the correlation length ξ which is a measure of the range of intermolecular spatial correlations. Thus, if the critical point is approached sufficiently closely, ξ will eventually become comparable to the system dimensions even though the range of intermolecular potentials involved does not exceed a few molecular diameters [1–3].

Consider, for instance, a fluid next to a solid surface (i.e., wall) when the thermodynamic state of the fluid pertains to the near-critical regime. This situation has recently received a lot of interest because of its relation to adsorption or wetting phenomena at solid-fluid interfaces [4–6]. In a seminal paper Fisher and de Gennes investigated the density profile of a semiinfinite near-critical fluid adsorbed on a single planar wall [6]. From an analysis of the density profile Fisher and de Gennes conjectured that under these circumstances the surface excess concentration Γ varies as $t^{-(\nu-\beta)}(\nu-\beta \cong 0.3)$ in the limit $t \to 0$ where $t = (T - T_c)/T_c$ (T, T_c actual and critical temperature, respectively).

While ξ may increase without limit in the semi-infinite model just described, a limit is posed to its growth if the system is confined in one or more dimensions, a situation which arises, for example, if a fluid is adsorbed in colloidal or porous adsorbents. Here it is conceivable that a near-critical regime exists in which ξ would exceed the size of microscopic or mesoscopic spaces to which the system is confined so that its criticality will be affected by confinement. The impact of confinement on criticality has been investigated by Fisher and Nakanishi who considered an Ising magnet confined in one dimension by an external potential (slit-pore geometry) [7,8]. They find a shift of the critical point as well as of the entire coexistence curve of the confined magnet with respect to a corresponding bulk system. Critical-point shifts of this sort have also been reported by Thommes and Findenegg who determined experimentally the phase behavior of fluid SF_6 adsorbed in a mesoporous medium [9].

However, the nature of critical adsorption of fluids in colloidal and porous adsorbents is still an open question. For example, Γ has been measured for a system of SF_6 in a colloidal (Vulcan 3-G graphitized carbon black) and a mesoscopic porous medium (controlled-pore glass, mean pore width around 30 nm) along near-critical isochores [10,11]. A remarkable behavior is observed: for $T \gg T_c$ Γ increases weakly with decreasing temperature, as ex-

*Author to whom correspondence should be addressed.

pected. Sufficiently close to T_c this temperature dependence appears to be inverted: Γ decreases sharply, contrary to the expected behavior [11].

To understand the temperature dependence of Γ, an analysis at the microscopic level is indispensable, which motivated the present work. As we will demonstrate, the mechanism underlying the decrease of Γ in the near-critical regime is rather complex. Thus, we are tempted to investigate critical adsorption in sufficiently realistic models which can be employed only in computer simulations. Relevant model systems are introduced in Sec. II. To mimic the experimental conditions, also to be described briefly in Sec. II, as closely as possible in parallel simulations, the grand canonical ensemble Monte Carlo (GCEMC) method is most apt. Section III is devoted to a presentation of the results. In Sec. IV we present a plausibility argument based upon a simple two-fluid van der Waals model to interpret our results. The paper concludes in Sec. V with a summary and discussion of our findings, with particular emphasis on a molecular explanation of the experimental results [11].

II. COMPUTATIONAL ASPECTS AND RELEVANT MODEL SYSTEMS

In a series of key experiments, Thommes and Findenegg investigated sorption of a pure fluid (SF_6) in a controlled-pore glass (CPG) which is a mesoporous medium consisting basically of cylindrical pores of a mean pore width of around 30 nm [11]. The surface excess amount Γ is measured as a function of temperature along near-critical isochores using a volumetric technique. The experimental setup consists of a reference cell of fixed volume containing the fluid at the density of the isochore to be considered and an adsorption cell with variable volume in which a bulk fluid reservoir is in contact with the CPG material. The pressure difference between the two cells is monitored by a sensitive differential pressure transducer. Measurements start at a temperature well above T_c at which the fluid density in the adsorption and reference cells is adjusted by varying the volume of the former until $\Delta P=0$. As T is now lowered, a pressure difference ΔP between the two cells builds up due to sorption of fluid by the substrate. At each temperature the original density of the bulk reservoir is restored by changing the volume of the adsorption cell until again $\Delta P=0$. Changes in the surface excess amount are given in terms of volume changes of the adsorption cell (see [9,11] for details).

The most striking effect observed experimentally under these conditions is the already mentioned sharp decrease of Γ if $T\rightarrow T_c+$ [11]. The microscopic structure of the fluid associated with this phenomenon is the focal point of the remainder of this article. To address it we view SF_6 in the bulk reservoir and in the pores as open subsystems in thermodynamic equilibrium with each other. This renders GCEMC simulations computationally sensible in which the condition of thermodynamic equilibrium is automatically observed by fixing chemical potential μ and temperature T as input parameters to the same value in both subsystems [12–14]. Since depletion was found not only with the porous glass but also with a colloidal graphite substrate [11], it was conjectured that it should not depend on details of the pore geometry. In the simulations it is then convenient to employ a model of a mesoscopic slit pore in which a fluid of N structureless spherically symmetric molecules is confined between two plane-parallel walls separated by a distance s_z along the z axis of the (Cartesian) coordinate system. The walls are perfectly smooth in the transverse (x,y) directions, that is, they lack entirely any distinct crystallographic structure. This is not unreasonable in view of the experimental situation where the silicate structure of CPG bears no particular resemblance to the molecular structure of SF_6 which may be perceived as a spherically symmetric molecule.

According to its geometry the configurational energy of our pore model can be written as a sum of three terms, namely,

$$U=U_{\mathrm{FF}}+U_{\mathrm{FW}}^{(1)}+U_{\mathrm{FW}}^{(2)}\ , \tag{1}$$

where the subscripts refer to fluid-fluid (FF) and fluid-wall (FW) interactions, respectively; the superscripts denote interactions between fluid molecules and lower$^{(1)}$ and upper$^{(2)}$ wall, respectively. We take

$$U_{\mathrm{FF}}=\sum_{i=1}^{N-1}\sum_{j=i+1}^{N}u_{\mathrm{FF}}(r_{ij})\ , \tag{2}$$

where

$$u_{\mathrm{FF}}(r_{ij})=4\varepsilon_{\mathrm{FF}}\left[\left[\frac{\sigma}{r_{ij}}\right]^{12}-\left[\frac{\sigma}{r_{ij}}\right]^{6}\right] \tag{3}$$

is the Lennard-Jones (LJ) (12,6) potential. $\varepsilon_{\mathrm{FF}}$ is the well depth, σ the molecular "diameter" and $r_{ij}=|\mathbf{r}_i-\mathbf{r}_j|$ denotes the distance between molecules i and j located at $\mathbf{r}_i$ and $\mathbf{r}_j$, respectively. In corresponding bulk reservoir simulations (Sec. III A) U is given by the first summand and on the right hand side of Eq. (1). Similarly,

$$U_{\mathrm{FW}}^{(k)}=\sum_{1}^{N}u_{\mathrm{FW}}(z_i^{(k)})\ , \tag{4}$$

where $z_i^{(k)}=|z_i-z^{(k)}|$ denotes the distance between molecule i and wall k located at $z^{(k)}/s_z=\pm 0.5$.

We consider two different model potentials to ascertain the effect of their analytic form on the microscopic structure of the adsorbed fluid. Model A, which is often used in MC simulations of adsorption [15], assumes the walls to consist of N_s solid atoms "smeared" over a *single* square plane of area s^2. If these atoms are supposed to interact with each fluid molecule via the LJ (12,6) potential, one has

$$u_{\mathrm{FW}}^{A}(z_i^{(k)})=2\pi\varepsilon_{\mathrm{FW}}d_s\sigma^2\left[\frac{2}{5}\left[\frac{\sigma}{z_i^{(k)}}\right]^{10}-\left[\frac{\sigma}{z_i^{(k)}}\right]^{4}\right]+u_{\mathrm{HW}}(z_i^{(k)})\ , \tag{5}$$

where $\varepsilon_{\mathrm{FW}}$ denotes the well depth $d_s=N_s/s^2$ and the solid atoms are of the same size as a fluid molecule. Equation (5) results from Eq. (3) by averaging $u_{\mathrm{FF}}(r_{ij})$

over x_j and y_j while holding $\mathbf{r}_i$ (the position of a fluid molecule) fixed and by adding a hard-wall background potential

$$u_{\mathrm{HW}}(z_i^{(k)})=\begin{cases}0, & z_i^{(k)}>0\\ \infty, & z_i^{(k)}=0\end{cases}, \tag{6}$$

to render the pore volume $V=s_z s^2$ unambiguous [12]. u_{FW}^{A} is a typical *short-range* potential. However, it ignores the fact that in experimental systems the (three-dimensional) walls are composed of a large number of crystallographic planes separated by some distance Δ which is determined by the crystallographic structure and the lattice constant. Thus, we introduce model *B*, for which

$$u_{\mathrm{FW}}^{B}(z_i^{(k)})=u_{\mathrm{FW}}^{A}(z_i^{(k)}) - \frac{2\pi}{3}\varepsilon_{\mathrm{FW}} d_s \sigma^2 \left[\frac{\sigma}{z_i^{(k)}+0.61\sigma}\right]^3 . \tag{7}$$

The second term on the right hand side of Eq. (7) represents the field exerted by an infinite number of crystallographic planes on a fluid molecule approaching the walls' surfaces where $\Delta=\sigma$ is assumed for simplicity. On account of the additional term $\propto (z_i^{(k)})^{-3} u_{\mathrm{FW}}^{B}$ incorporates *long-range* attractive fluid-wall interactions.

To enable a quantitative discussion below, it is useful to introduce the parameter

$$f=\frac{\pi d_s \sigma^2}{2}\frac{\varepsilon_{\mathrm{FW}}}{\varepsilon_{\mathrm{FF}}}, \tag{8}$$

which is a measure of the *relative* strength of fluid-wall interactions. For the results in this paper we choose $d_s^*=0.782\,717$ ($f=1.2295$, $\varepsilon_{\mathrm{FW}}/\varepsilon_{\mathrm{FF}}=1.0$) (see Table I, Sec. III B). Henceforth we follow common practice and express quantities of interest in terms of the LJ (12,6) parameters $\varepsilon_{\mathrm{FF}}$ and σ or appropriate combinations of the two [13]. These dimensionless quantities are denoted by an asterisk. We use periodic boundary conditions and the minimum image convention in all three (bulk reservoir, Sec. III A) or x,y (slit-pore, Sec. III B) directions [13]. The simulations employ the Taylor-expansion algorithm recently proposed by one of us [14] to reduce substantially the computational effort required to generate a numerical representation of a Markov chain of configurations. Computational efficiency is a particularly important aspect as far as simulations in the near-critical regime are concerned. Due to (physically significant) large fluctuations, averages are prone to inacceptably large statistical errors for typical run lengths of $\leq 10^6$ GCEMC steps normally employed in computer simulations of non- (i.e, sub- or super-) critical thermodynamic states. The aspect of statistical accuracy was noted and investigated in depth by van Megen and Snook, who focused in particular on the pore average density obtained in GCEMC simulations of a near-critical fluid confined to a smooth-wall slit pore [16]. By applying statistical tests to the particle-number distribution and taking into account in particular its "skewness" (defined in terms of the second and third moments of this distribution) as a measure of statistical accuracy, van Megen and Snook estimate an error of 1–2 % for their pore average density if it is averaged over 2×10^6 configurations (p. 633 in [16]). They also concluded that results for "simple" averages like density, energy, pressure, etc., are independent of simulation cell volumes V if $V^*\geq 125$ (p. 631 in [16]). Because of the system sizes used in the present work and the typical length of a GCEMC simulation which exceeds the ones reported by van Megen and Snook by a factor of 5 (see Table I), a smaller statistical uncertainty of $\leq 1.5\%$ is expected for the results presented below. This applies particularly to results for states in the immediate vicinity of the critical point ($T^*\leq 1.50$) which are based on 3–5 independent runs starting from different (random) configurations. Although to our knowledge van Megen and Snook's careful and detailed study is the only previous one dealing with near-critical phenomena in phases confined to smooth-wall mesoscopic slit pores, further comparison with their work is prevented because they studied adsorption along one *isothermal* path instead of an *isochoric* path. However, the more general remarks concerning appropriate conditions for GCEMC simulations in the near-critical regime still apply to our work.

TABLE I. Technical details of Monte Carlo simulations employing the Taylor expansion method [14].

Ensemble	Grand canonical
Starting configuration	random
Number of equilibration steps	3.5×10^5
Number of steps between subsequent averages	$2N-3N$
Total number of MC steps	10.0×10^6
Side length of simulation cell in the x-y plane s^*	7.9925
Side length of simulation cell in z direction s_z^*	20.0
Side length of displacement cube d_r^*	0.05–0.13
Surface density d_s^* of the walls	0.782 717
Radius of primary zone sphere r_1^*	1.8
Thickness of secondary zone cylindrical shell $\Delta r^*=r_2^*-r_1^*$ in the x-y plane	0.7
Radius of neighbor list r_N	2.7σ
Potential cutoff (pressures, energies, etc.) r_c	3.5σ

More recently, Recht and Panagiotopoulos have employed the Gibbs ensemble MC method to investigate artificial shifts of the location of the critical point in bulk Lennard-Jones and square-well fluids caused by the inevitable microscopic dimension of the simulation cell [17]. From their detailed study these authors concluded that for the three-dimensional Lennard-Jones fluid no systematic dependence of the critical-point location exists if the simulation cells contain more than 200 molecules. This situation is quite different if instead of the continuous three-dimensional Lennard-Jones fluid a *discrete* two-dimensional near-neighbor lattice gas is considered. For the latter model Mon and Binder report a shift of T_c to higher values with decreasing size of the simulation cell for both Gibbs ensemble MC and GCEMC [18].

III. RESULTS

A. Criticality of the bulk reservoir

To mimic the experiment subject to constraints of (a) thermodynamic equilibrium between bulk reservoir and adsorbed fluid in the adsorption cell and (b) adsorption along isochoric paths by varying $T \to T_c +$, we begin by determining $\mu = \mu(\rho_c, T \to T_c +)$ in a trial-and-error fashion for a number of temperatures by varying μ at $T = \text{const}$ in individual GCEMC runs. The results for a series of temperatures listed in Table II deviate from the mean $\bar{\rho}^* = 0.365$ by less than 1.0%. This value is in close agreement with $\rho_c^* = 0.36$ given by Hansen and Verlet [19].

To test consistency of our results, the pressure P

$$\frac{\beta P}{\rho} = 1 - \frac{1}{3N} \left\langle \sum_{i=1}^{N-1} \sum_{j=i+1}^{N} \nabla_{ij} U \cdot \mathbf{r}_{ij} \right\rangle + \frac{\beta P_{\text{corr}}}{\rho} \tag{9}$$

is computed via Clausius' virial theorem [20], where $\beta = (k_B T)^{-1}$ and P_{corr} is a correction due to the potential cutoff (see Table I) which may be computed analytically. An explicit expression is presented in [21] based upon the assumption of a random distribution of molecules j around any reference molecule i given a sufficiently large cutoff. Results listed in Table II are plotted versus T in Fig. 1. It turns out that the temperature dependence of P can well be approximated by a straight line as one would expect, for instance, for a van der Waals fluid along an isochoric path. Fitting the van der Waals equation of state

$$P = \frac{\rho}{1 - \rho b} k_B T - a\rho^2 , \tag{10}$$

by a linear least-squares procedure to the data in Table II, the straight line in Fig. 1 is obtained. The fit also permits us to compute the van der Waals constants a and b and with them critical values of temperature $T_c^* = 1.38$ and pressure $P_c^* = 0.134$ are estimated which are well within the range of values reported for the LJ (12,6) fluid [19,22–24]. In addition, we analyze structural characteristics of the fluid manifested in the radial pair correlation function $g^{(2)}(r)$ which is defined as

$$g^{(2)}(r) = \frac{\langle N(r) \rangle}{4\pi r^2 \Delta r \rho} , \tag{11}$$

TABLE II. Chemical potential μ, pressure P, and bulk reservoir density ρ_b as functions of temperature T from GCEMC simulations of the homogeneous bulk reservoir Lennard-Jones (12,6) fluid. $\mu(T \to T_c +)$ is obtained in a trial-and-error fashion for a near-critical isochoric path subject to the condition $\rho_b(T) = \langle N \rangle / V \cong \rho_c$ (see Sec. III A).

T^*	$-\mu^*$	P^*	ρ_b^*
1.38	14.94	0.149	0.365
1.40	15.11	0.159	0.364
1.425	15.33	0.180	0.364
1.45	15.55	0.195	0.365
1.50	16.00	0.228	0.367
1.60	16.90	0.303	0.369
1.70	17.81	0.372	0.365
2.00	20.63	0.577	0.368

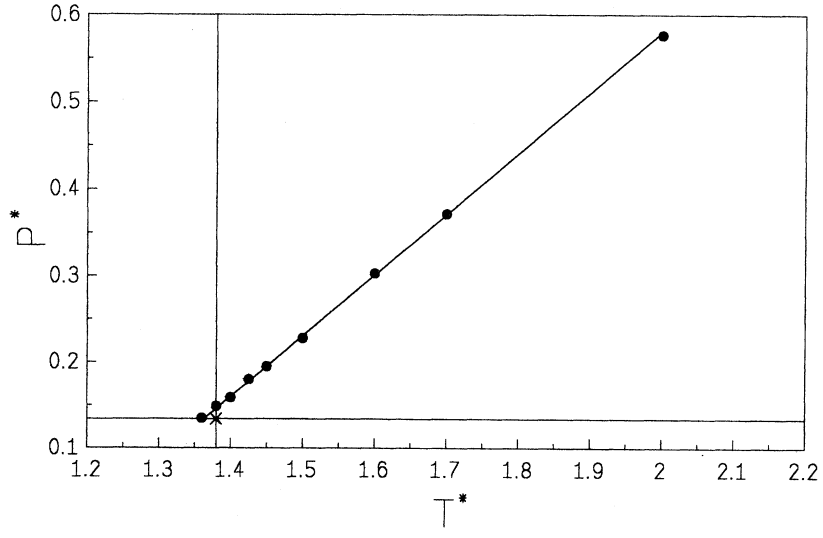

FIG. 1. The pressure P^* as a function of temperature T^* of a homogeneous bulk fluid from GCEMC simulations in which the chemical potentials $\mu(T)$ have been chosen according to the condition $\bar{\rho}^*(T) = 0.365 \cong \rho_c^*$. $\bar{\rho}^*(T)$ is the average density obtained by averaging over the entries listed in Table II. The solid line represents a fit of the van der Waals equation of state to the simulation data (see Sec. III A). Also shown is the location of the critical point obtained from the fit (X) at the intersection of the horizontal and vertical lines.

where $\langle N(r)\rangle$ is the number of molecules in a spherical shell of radius r and thickness Δr centered on a reference molecule. Angular brackets denote an ensemble average over a sufficiently large number of (statistically uncorrelated) configurations (see Table I) considering each molecule in a particular configuration as a reference molecule which is subsequently included in the averaging process. By standard textbook arguments one can furthermore show that in the grand canonical ensemble [25]

$$\rho\beta^{-1}\kappa_T = 1+\rho\int_V [g^{(2)}(\mathbf{r})-1]d\mathbf{r} \propto \langle N^2\rangle - \langle N\rangle^2 = \sigma_N^2 , \tag{12a}$$

where σ_N^2 is the variance of the particle-number distribution which is a direct measure of particle-number fluctuations. Thus, the characteristic divergence of the isothermal compressibility $\kappa_T \to \infty$ at the critical point can be attributed to diverging particle-number (i.e., density) fluctuations but also to long-range spatial correlations, i.e., a limiting behavior of [25]

$$\lim_{t\to 0} g^{(2)}(r) \propto \lim_{t\to 0} \frac{\exp(-r/\xi)}{r^{1+\eta}} = \frac{1}{r^{1+\eta}} , \quad \xi \propto t^{-\nu} \tag{12b}$$

where η and ν denote critical exponents. Plots of $g^{(2)}(r)$ in Fig. 2 reveal the expected long-range correlations in the near-critical regime: for a thermodynamic state representative of the near-critical regime $g^{(2)}(r)$ appears to be shifted slightly but significantly to values larger than 1.0. As expected from Eqs. (12a) this shift is the more pronounced the closer T is to T_c and is detected for temperatures $T^* \leq 1.60$. Thus, in the model system these lower-temperature states belong to the near-critical regime. However, it is noteworthy that this temperature range appears to be extended compared with experimental systems. Even though long-range correlations seem rather weak and are superimposed to short-range correlations (caused by intermolecular interactions) for $r^* < 4.0$, the "tail" in $g^{(2)}(r)$ indicative of the fluid's criticality appears to decay nearly negligibly within the range of intermolecular separations accessible. Via Eq. (12a) a "tail" in $g^{(2)}(r)$, however small, gives rise to the characteristic divergence of κ_T in a sufficiently large system. If, on the other hand, the temperature is well outside the near-critical regime, $g^{(2)}(r)$ exhibits only short-range correlations which do not exceed the third neighbor shell ($r^* \cong 3.0$) because of packing characteristics of fluid molecules at the relatively low density $\bar{\rho}^* = 0.365$. This can also be seen in Fig. 2 where $g^{(2)}(r)$ does not have any tail at $T^* = 2.00$.

B. Microscopic structure of the pore fluid

Having determined $\mu(\rho_c, T \to T_c+)$ for the bulk fluid reservoir, we are now in a position to proceed with parallel GCEMC simulations for the pore fluid. Since we intend to investigate the confined fluid's microscopic structure, the local density

$$\rho^{(1)}(z) = \frac{\langle N(z)\rangle}{s^2\Delta z} \tag{13}$$

is the simplest quantity to deliver that information. $N(z)$ is the number of molecules in a thin layer of thickness Δz parallel to the walls and centered on z. In general, the local density depends on the (vector) position $\mathbf{r}$ of a molecule with respect to the walls. However, because of the external field's (represented by the walls) symmetry in models A and B, $\rho^{(1)}(z)$ depends only on its scalar argument z [26]. $\rho^{(1)}(z)$ is symmetric with respect to the plane centered at $z^* = 0.0$. Plots of $\rho^{(1)}(z)$ are therefore always shown only in the lower half of the pore space ($-0.5 \leq z/s_z \leq 0.0$) and are averaged over symmetrically equivalent points in the regimes $z \leq 0$ and $z \geq 0$.

We begin by considering model A and choose $s_z^* = 20.0$ throughout and $f = 0.984$ ($\varepsilon_{FW}/\varepsilon_{FF} = 0.8$) [see Eq. (8)] to represent a mesoporous material in which the strengths of fluid-fluid and fluid-wall interactions are nearly equal. In Fig. 3, plots of $\rho^{(1)}(z)$ are presented corresponding to these settings and for three selected temperatures, $T^* = 1.36$, 1.45, and 3.00. Regardless of T, $\rho^{(1)}(z)$ exhibits an oscillatory structure in the vicinity of the walls that reflects layering of fluid molecules. Layering is a direct consequence of fluid-wall interactions [27] and apparently does not persist for distances $|z_i^{(k)*}| \geq 3.0$ from either

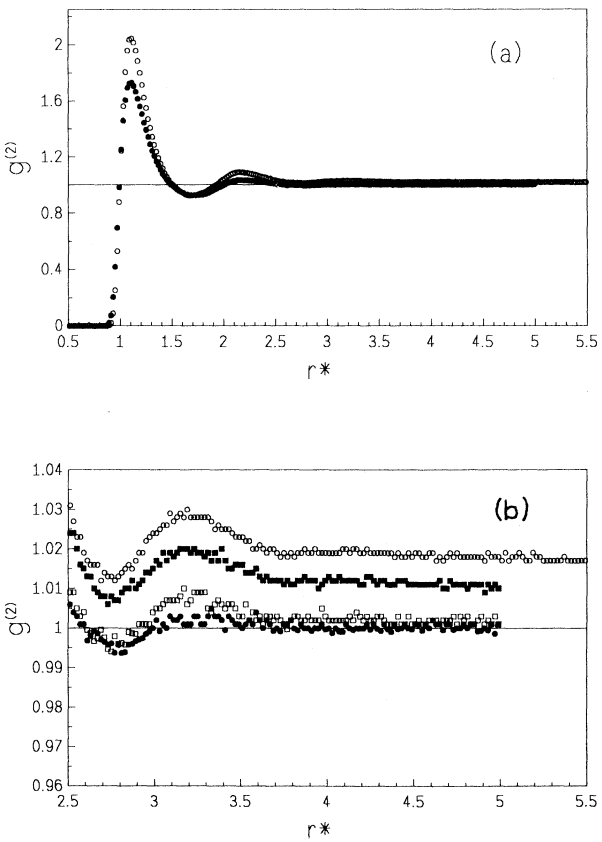

FIG. 2. The radial pair correlation function $g^{(2)}(r)$ as a function of intermolecular separation r^* for a homogeneous bulk fluid at $\rho^* = 0.365 \cong \rho_c^*$. (a) $T^* = 1.36 \cong T_c^*$ (○); $T^* = 2.00$ (●). (b) The same as (a) but on enhanced scales to demonstrate the fluid's criticality. In addition, results for $T^* = 1.45$ (■) and $T^* = 1.60$ (□) are also shown in (b).

wall. This is not surprising because for $|z_i^{(k)*}| \geq 3.6$ ($|z_i^{(k)}|/s_z = 0.18$), $u_{\mathrm{FW}}^{A}(z_i^{(k)})$ is less than 1.0% of its minimum value. Thus, it is reasonable to define a *wall* region $-0.5 \leq z/s_z \leq -0.32$ in which the fluid's (normal) structure is dominated by fluid-wall interactions and a *core* region $-0.32 \leq z/s_z \leq 0.00$ in which fluid-wall interactions are negligible. Note that the envelope of $\rho^{(1)}(z)$ in the wall region exceeds by far the bulk critical density ρ_c that is, under the present conditions the fluid is adsorbed by the walls.

In the wall region the extent of layering (i.e., adsorption) diminishes with increasing T which is reflected by a decreasing peak height in $\rho^{(1)}(z)$. This is due to the higher (average) kinetic energy of fluid molecules at higher T which enables them to "escape" the regime of attractive fluid-wall interactions more easily. In the corresponding core region nothing spectacular is observed as far as thermodynamic states well off the near-critical regime (i.e., $T^* \geq 1.60$) are concerned: the core region density is constant at $\rho \cong \rho_c$, that is the core region is homogeneous and its properties are therefore identical to those of the bulk reservoir in thermodynamic equilibrium with it. This is expected because core fluid properties are dominated by fluid-fluid interactions.

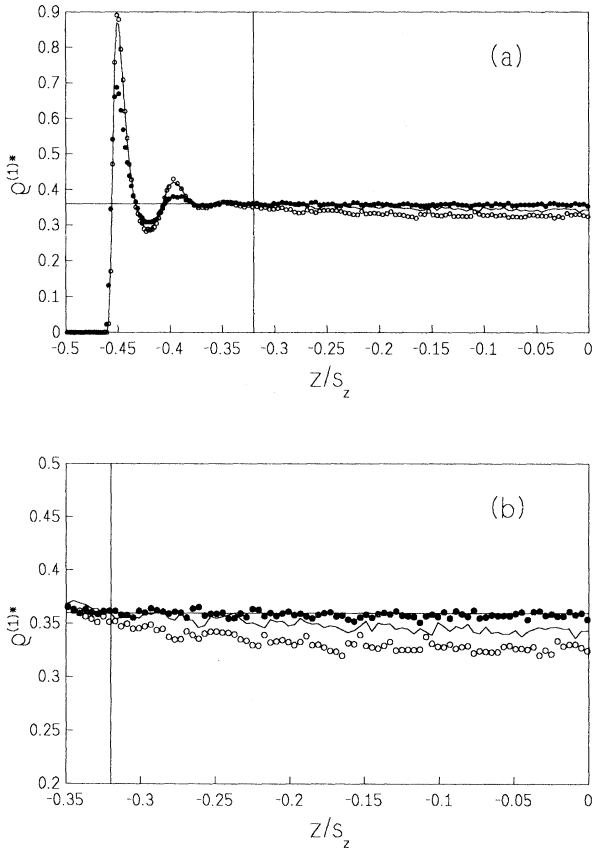

FIG. 3. The local density $\rho^{(1)*}(z)$ as a function of position z in a mesoporous slit-pore ($s_z^* = 20$, model A, $f = 0.9836$). For reasons of symmetry (see text) only the lower half of the pore space is shown. (a) $T^* = 1.36 \cong T_c^*$ (○); $T^* = 1.45$ (——); $T^* = 3.00$ (●). The *horizontal* solid line represents the constant bulk reservoir density $\rho^* = 0.365 \cong \rho_c^*$. The *vertical* solid line represents the range of the fluid-wall interaction potential (see Sec. III B for a definition). (b) The same as (a) but on enhanced scales to demonstrate depletion in the core region of the pore.

However, a surprising phenomenon is observed for states belonging to the bulk near-critical regime (i.e., $T^* < 1.60$): the core region appears to be depleted with respect to the bulk density ρ_c. Depletion is more pronounced the larger the distance of a reference point from both walls. The *entire* cross section of the pore is thus inhomogeneous compared with noncritical states where inhomogeneity is restricted to the wall region. Depletion also becomes more pronounced as T_c is approached more closely. This is obvious from Fig. 3(b), where the negative deviation of $\rho^{(1)}(z)$ from ρ_c in the core region is larger the closer T is to T_c. It is furthermore emphasized that because of adsorption at the walls, depletion must not be confused with a drying phenomenon (see also Sec. V). Instead, depletion should be perceived as a novel phenomenon pertaining to the bulk near-critical regime. This is concluded from Fig. 3 and is furthermore corroborated by Fig. 4, where $\rho^{(1)}(z)$ is plotted for $T^* = 1.36 \cong T_c^*$ and $\mu^* = -14.75, -15.00$, the latter corresponding to a subcritical density $\rho_b^* = 0.345 \cdot \rho_c^*$. Thus depletion is not expected, should adsorption be carried out in a mesoporous medium along a noncritical bulk isochore where ξ is small compared with the pore dimensions and varies comparatively weakly with T (cf. Fig. 4).

To ascertain the influence of intermolecular interactions on the depletion phenomenon, we begin by investigating the effect of the analytic form of the fluid-wall potential and employ model B, which is known to provide a more realistic representation of the walls [28–30] as far as models of specific experimental systems are concerned. The major difference between models A and B is an additional attractive contribution proportional to $(z_i^{(k)})^{-3}$ present only in the latter (see Sec. II). Plots in Fig. 5 reveal that depletion occurs in both models while the fluid is still adsorbed by the walls. In fact, by adjusting f properly the extent of depletion can be made nearly the same for both models (see Fig. 6). Because of the additional attractive contribution, f must be smaller for model B. Since we refrain from engaging in a quantitative comparison between experiment and simulation and wish to focus solely on qualitative aspects of the depletion phenomenon, we conclude from Figs. 3–6 that the somewhat simpler model, A, suffices under the present conditions.

Since, on the other hand, the relative strength of the fluid-wall interaction does affect the extent of depletion (see Fig. 6), it seems worthwhile to investigate the influence of f on it in more detail. Therefore, we present in Fig. 7 the average pore density $\rho_p = \langle N \rangle / s^2 s_z$ as a function of f for two different temperatures $T^* = 1.36 \cong T_c^*$ and $T^* = 1.60$. Both data sets can be well approximated by linear least-squares fits and reveal markedly different slopes. The latter seems plausible because at $T^* = 1.60$ the (relatively small) wall region is predominantly affected by variations in f, leaving the core-region density at $\rho_{\mathrm{core}}^{(1)}(z) \cong \rho_c = \text{const}$. On the contrary, both core and wall regions are affected simultane-

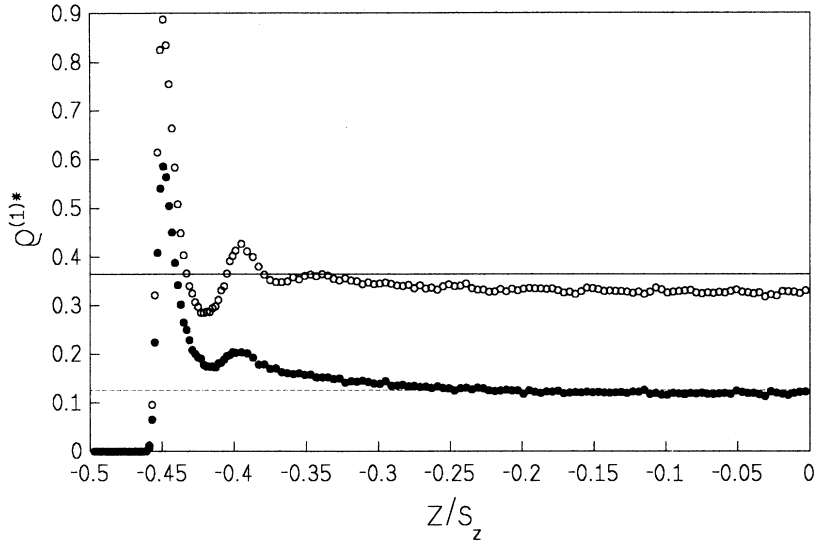

FIG. 4. The local density $\rho^{(1)*}(z)$ as a function of position z in a mesoporous slit-pore ($s_z^*=20$, model A, $f=0.9836$, $T^*=1.36\cong T_c^*$). $\mu^*=-14.75$ (○) corresponding to a bulk reservoir density of $\rho^*=0.365\cong\rho_c^*$ (——); $\mu^*=-15.00$ (●) corresponding to a bulk reservoir density of $\rho^*=0.345\times\rho_c^*$ (— — —).

ously at $T^*=1.36$ (see Figs 3 and 5). Due to their different slopes, a value $f_{\text{inter}}=1.201$ exists at which the two fits intersect. Based upon the value of f_{inter}, two classes of systems are discernible. For $f<f_{\text{inter}}$, depletion is expected as ρ_p decreases with $T\to T_c+$. The corresponding plots in Fig. 8 indicate that in the core region $\rho^{(1)}(z)$ does not approach ρ_c, but a distinctly smaller value, which turns out to be smaller the smaller f is. From the form of $\rho^{(1)}(z)$ we conclude that for sufficiently low values of f, drying at the walls is superimposed and enhances depletion. The form of $\rho^{(1)}(z)$ in the presence of drying ($f=0.0615$, see Fig. 8) is qualitatively similar to results obtained by density functional theory for weak fluid-substrate interactions [31] and by integral-equation methods [32]. However, models in which drying dominates strongly are regarded as inappropriate with respect to the experimental situation [11]. For $f>f_{\text{inter}}$ the temperature dependence of ρ_p is inverted, that is ρ_p increases as $T\to T_c+$. This latter class does not exhibit depletion as can be seen in Fig. 8: instead $\rho^{(1)}(z)$ approaches ρ_c from above. Thus, the relative strength of the fluid-wall interaction should not exceed a certain threshold for depletion to occur in the near-critical regime of thermodynamic states. The precise value of the threshold depends on details of the model and on s_z in particular. Thus, depletion depends on a subtle interplay between s_z and f_{inter} [33].

Finally, we wish to delve a little bit deeper into the microscopic structure of confined near-critical fluids by considering the *in-plane* pair correlation function

$$g^{(2)}(z_1,\rho_{12})=\frac{\langle N(z_1,\rho_{12})\rangle}{2\pi\rho_{12}\Delta\rho_{12}\Delta z\bar{\rho}^{(1)}(z_1)}\ , \tag{14a}$$

where $\langle N(z_1,\rho_{12})\rangle$ is the average number of molecules in an annulus of radius ρ_{12}, width $\Delta\rho_{12}$, and height Δz around a reference molecule located at z_1. To achieve normalization [i.e., $\lim_{\rho_{12}\to\infty}g^{(2)}(z_1,\rho_{12})=1$ for noncritical thermodynamic states] the average density of the annulus

$$\bar{\rho}^{(1)}(z_1)=\frac{1}{\Delta z}\int_{z_1-\Delta z/2}^{z_1+\Delta z/2}\rho^{(1)}(z)dz \tag{14b}$$

needs to be incorporated in the denominator of Eq. (14a). Thus, $g^{(2)}(z_1,\rho_{12})$ is a measure of *transverse* structure (i.e., structure parallel with the walls) whereas $\rho^{(1)}(z)$ pro-

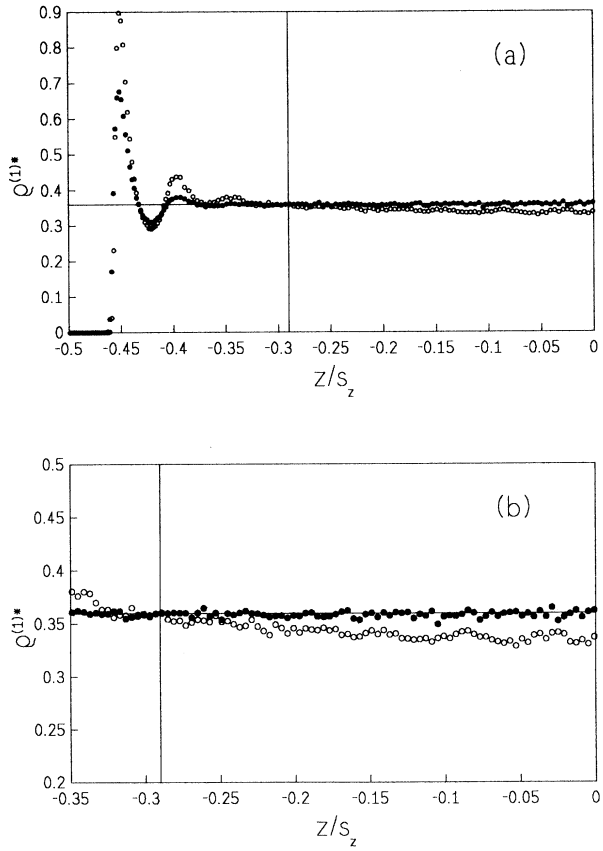

FIG. 5. Same as Fig. 3, but for model B and $f=0.860\,65$. Results are shown only for two temperatures $T^*=1.36\cong T_c^*$ (○); $T^*=3.00$ (●).

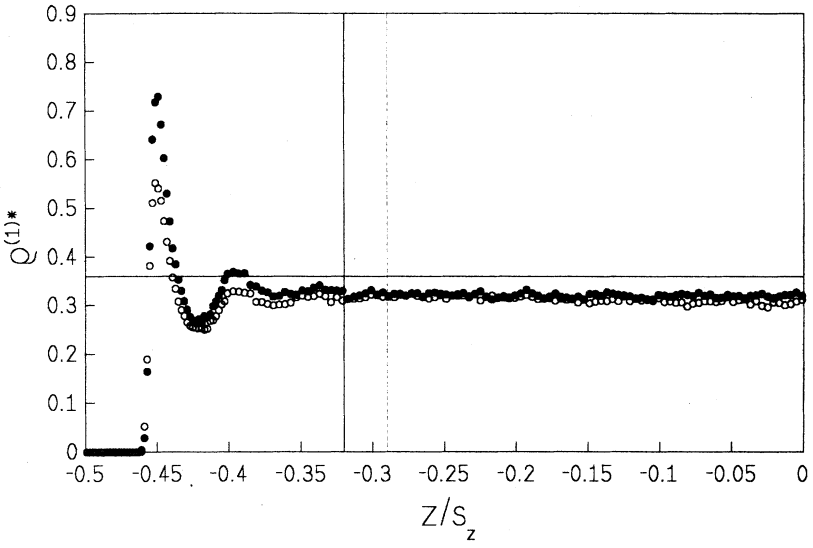

FIG 6. The local density $\rho^{(1)*}(z)$ as a function of position z in a mesoporous slit-pore ($s_z^*=20$, $T^*=1.36\cong T_c^*$). Model A ($f=0.8607$) (●), model B ($f=0.6148$) (○). The solid *horizontal* line represents the bulk reservoir density $\rho^*=0.365\cong\rho_c^*$. The *vertical* lines represent the ranges of the fluid-wall interaction potentials of model A (——) and model B (— — —) (see Sec. III B).

vides information about the fluid's *normal* structure. $g^{(2)}(z_1,\rho_{12})$ has been proven to be particularly useful in analyzing the structure of condensed phases in slit pores if one restricts its evaluation to reference molecules with $\{z_1\}$ all belonging to the same layer [i.e., the same peak of $\rho^{(1)}(z)$]. Then Δz denotes the distance between the minima enclosing a peak of $\rho^{(1)}(z)$ and the evaluation of $g^{(2)}(z_1,\rho_{12})$ for a succession of layers with increasing distance from the walls provides direct information about the variation of lateral order [12,26,27]. In the present context $g^{(2)}(z_1,\rho_{12})$ cannot be associated with individual layers in the core region (see Figs. 3 and 5). To investigate variations of lateral order we evaluate $g^{(2)}(z_1,\rho_2)$ for molecules located in the *contact layer* [corresponding to the peak of $\rho^{(1)}(z)$ closest to the wall] and a thin *virtual* layer of thickness $\Delta z^*=1.0$ centered on $z^*=0.0$. For two representative temperatures $T^*=1.36\cong T_c^*$ and $T^*=2.00$ we plot $g^{(2)}(z_1,\rho_{12})$ in Figs. 9 and 10 as functions of intermolecular separation for wall and core regions, respectively. At the lower temperature $g^{(2)}(z_1,\rho_{12})$ for the core region exhibits long-range correlations similar to the ones presented in Fig. 2. Although statistical accuracy is necessarily lower than for $g^{(2)}(r)$, $g^{(2)}(z_1,\rho_{12})$ is again significantly larger than 1.0 for all intermolecular separations accessible. Long-range correlations are, however, not observed in the wall region where fluid-wall interactions dominate. Plots of the corresponding $g^{(2)}(z_1,\rho_{12})$ in Fig. 9 indicate a loss of almost all correlations for intermolecular separations $\rho_{12}^*>2.5$. If, on the other hand, the thermodynamic state is well outside the near-critical regime (i.e., $T^*\geq 1.60$) the corresponding $g^{(2)}(z_1,\rho_{12})$'s are "well behaved," that is, they decay to one within $\rho_{12}^*<3.0$ in both wall *and* core regions (see Fig. 10). Thus, at sufficiently high temperatures no structural signature of near criticality is detected, which is consistent with the above observations concerning $\rho^{(1)}(z)$.

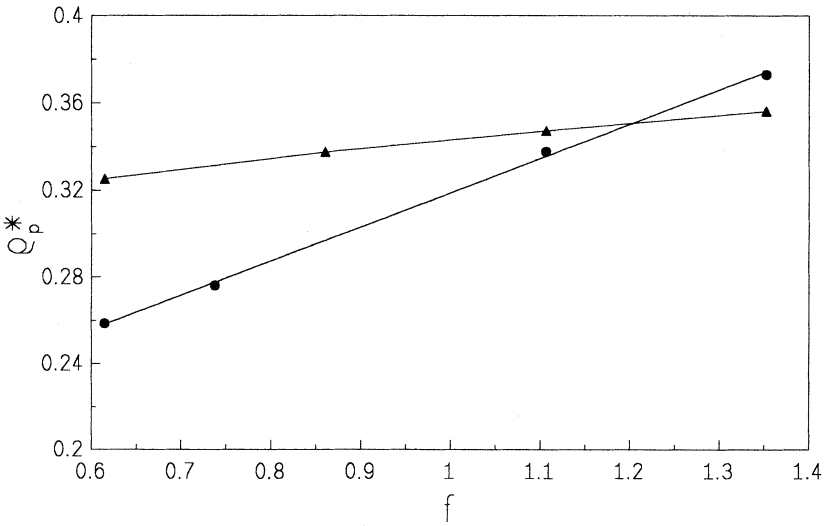

FIG. 7. The pore average density ρ_p^* as a function of the relative strength of the fluid-wall interaction potential f for model A at $T^*=1.36\cong T_c^*$ (●) and at $T^*=1.60$ (▲). The straight lines represent linear least-squares fits to guide the eye.

IV. DEPLETION AND RESTRICTED DENSITY FLUCTUATIONS

The GCEMC simulations discussed in the preceding sections provide clear evidence that under favorable conditions depletion in the core region of a mesoscopic pore occurs if the critical point of a pure bulk fluid is approached from *above*. Nakanishi and Fisher investigated order parameter profiles for an Ising magnet in a mesoscopic slit pore with attention to the example of phase separation in confined binary fluid mixtures [8]. They found that near criticality the order parameter at the center of the pore (midpoint value) is negative with respect to the bulk value. However, in Nakanishi and Fisher's work the critical point is approached from *below*. Thus, to understand depletion if the critical point of a pure fluid is approached from *above*, we present here a plausibility argument that suggests a simple mechanism. Let us consider a composite system consisting of an infinitely large bulk reservoir in thermodynamic and mechanical equilibrium with a fluid confined between two parallel walls. The distance s_z between the walls is assumed to be sufficiently large that a core region may be defined in which the fluid is homogeneous at the bulk density, provided T is high enough. Since depletion occurs only in the core region, we simplify our argument by considering only the core region explicitly; the remainder of the pore, namely, the walls and the fluid adsorbed by them (i.e., the wall region) is treated only implicitly: the wall region may act upon the core fluid as a mean external field if ξ is large enough that the field may be transmitted across an appreciable portion of the core fluid by means of density fluctuations.

Let us now subject bulk and core fluid to a gedanken experiment in which we lower T along the critical isochore starting from a sufficiently high value so that $\rho_{\text{core}}=\rho_{\text{bulk}}=\rho_{c,\text{bulk}}$ and $\xi_{\text{core}}=\xi_{\text{bulk}}$. Eventually a threshold temperature T_0 will be reached at which $\xi_{\text{core}}=O(s_z)$. The two subsystems are now separated and the temperature is lowered by dT, that is, $T'=T_0-dT$ while maintaining $\rho_{\text{core}}=\rho_{c,\text{bulk}}=\text{const}$ Since $\xi_{\text{core}}=O(s_z)$ an inspection of Eq. (12a) reveals that $\kappa_{T,\text{core}}<\kappa_{T,\text{bulk}}$ because density fluctuations are suppressed in the core. What impact may the different compressibilities have? To answer this question one

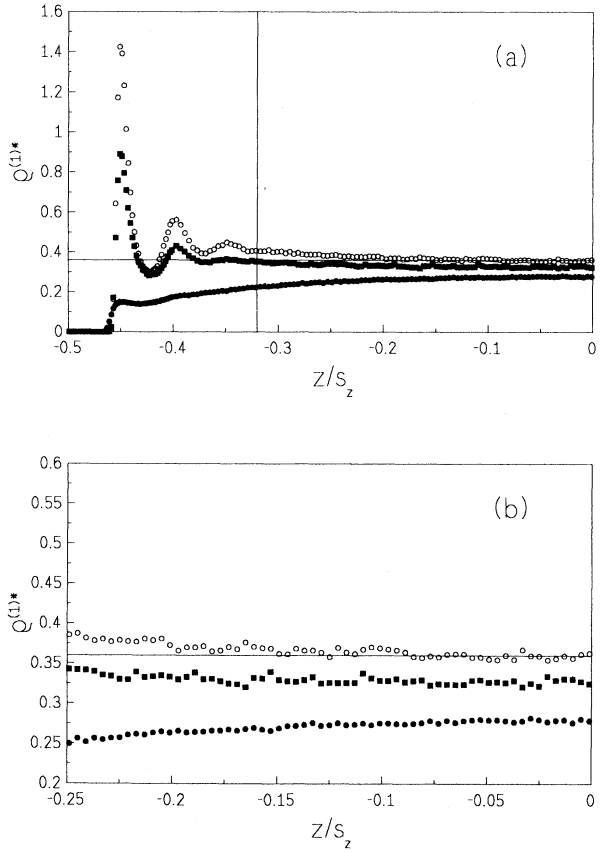

FIG. 8. The effect of the relative strength of the fluid-wall interaction potential f on the local density $\rho^{(1)}(z)$ (model A, $T^*=1.36\cong T_c^*$). (a) $f=0.0615$ (●), $f=0.9836$ (■), $f=1.3525$ (○). The *vertical* solid line represents the range of the fluid-wall interaction potential (see Sec. III B for a definition). (b) The same as (a) but on enhanced scales to demonstrate the effect in the core region of the pore.

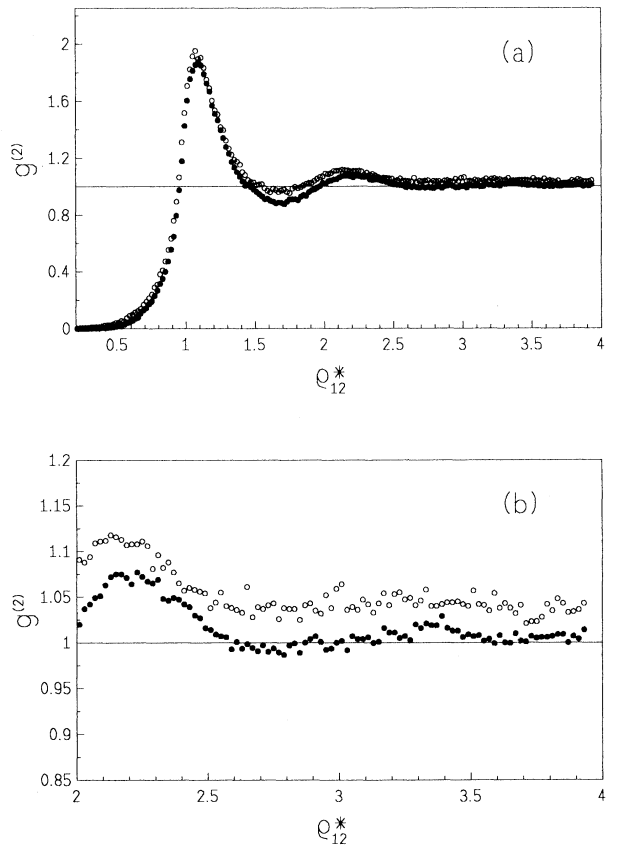

FIG. 9. The in-plane pair correlation function $g^{(2)}(z_1,\rho_{12})$ as a function of intermolecular separation ρ_{12}^* (model A, $f=0.9836$, $T^*=1.36\cong T_c^*$) for molecules located in the contact layer (●) and in a *virtual* layer centered on $z^*=0$ (○) (see Sec. III B). (b) The same as (a) but on enhanced scales to demonstrate the effect of the core fluid's criticality.

needs to establish an explicit relation between κ_T and other thermophysical properties, such as pressure P, for instance. Obviously, this program requires knowledge of an equation of state for bulk and core fluid. According to the results of Sec. III A it seems natural to adopt the van der Waals equation for the bulk fluid. Unfortunately, no such simple equation of state is available for the core fluid *a priori*. However, if one realizes that $T' \approx T_0$ at which bulk and core fluid were in the same thermodynamic state by definition, it seems permissible to employ the van der Waals equation for the core fluid at T', too. However, the molecular parameters a and b for the core fluid may differ from those for the bulk fluid because different compressibilities at the same T and ρ imply different critical points on account of confinement, in accord with other theoretical [8] assertions. In other words, at $T' < T_0$ the fluid in the core region is viewed as being *effectively* different from the bulk fluid. To proceed we rewrite Eq. (10) in a slightly different form as

$$\beta P = \rho \left[\frac{1}{1-\frac{1}{3}r} - \frac{9}{8} rt \right] , \tag{15a}$$

where $r = r_{\text{bulk}} = \rho/\rho_{c,\text{bulk}} = 1$ or $r = r_{\text{core}} = \rho/\rho_{c,\text{core}}$ and $t = T_{c,\text{bulk}}/T'$ or $T_{c,\text{core}}/T'$, respectively. Similarly, one has from Eq. (15a)

$$\beta \kappa_T^{-1} = \beta\rho \left[\frac{\partial P}{\partial \rho} \right]_{N,T} = \rho \left[\frac{1}{(1-\frac{1}{3}r)^2} - \frac{9}{4} rt \right] . \tag{15b}$$

Since we have made the transformation $T_0 \to T'$ along the critical isochore of the bulk fluid and because dT is infinitesimally small, we simplify Eqs. (15a) and (15b) for the core fluid by expanding the first terms in brackets in a Taylor series around $r_{\text{core}} = 1$, which yields

$$\begin{aligned} &\beta(\kappa_{T,\text{core}}^{-1} - \kappa_{T,\text{bulk}}^{-1}) \\ &\quad = \tfrac{9}{4}\rho_{c,\text{bulk}}[t_{\text{bulk}} - r_{\text{core}} t_{\text{core}} - (1 - r_{\text{core}})] \\ &\quad > 0 , \end{aligned} \tag{16a}$$

according to the foregoing discussion where we have also employed $r_{\text{bulk}} = 1$. Likewise one finds

$$\begin{aligned} \beta(P_{\text{core}} - P_{\text{bulk}}) = \tfrac{9}{8}\rho_{c,\text{bulk}}[&t_{\text{bulk}} - r_{\text{core}} t_{\text{core}} \\ &- \tfrac{2}{3}(1 - r_{\text{core}})] > 0 , \end{aligned} \tag{16b}$$

which must be positive because the right-hand side of Eq. (16a) is a positive quantity. Now suppose the subsystems are reconnected. Because of the pressure difference, matter must flow spontaneously from the core region into the bulk reservoir until the condition of mechanical stability $P_{\text{core}}(\rho_{\text{core}}, T') = P_{\text{bulk}}(\rho_{\text{bulk}}, T')$ at $\rho_{\text{core}} < \rho_{\text{bulk}}$ is reestablished. This suggests depletion as a phenomenon by which mechanical stability in a composite system is maintained if the correlation lengths of its constituents become different, an idea which we submit for further elaboration by one of the well-established theoretical approaches to critical-point phenomena.

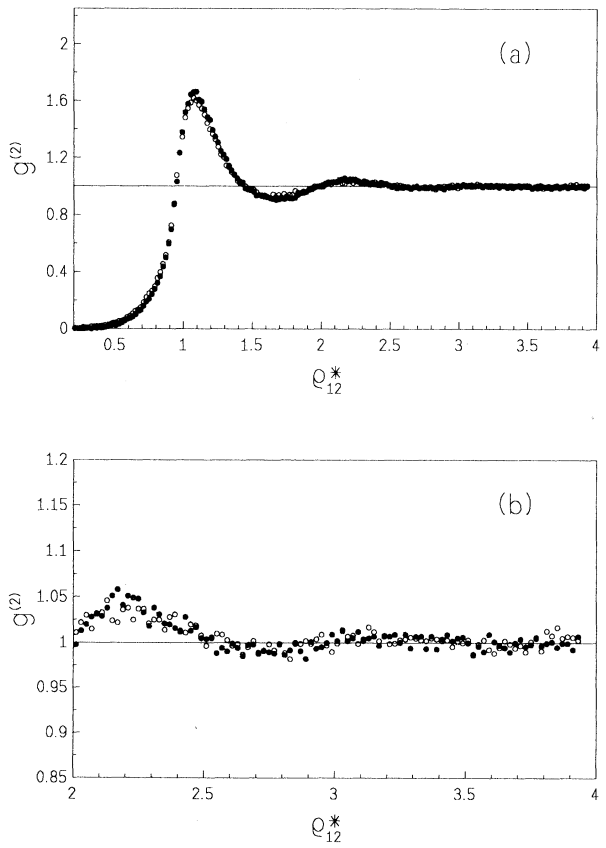

FIG. 10. (a) Same as Fig. 9(a), but for $T^* = 2.00$. (b) Same as (a), but on enhanced scales to demonstrate the noncritical character of the wall fluid.

V. DISCUSSION AND CONCLUSIONS

In this article we analyze the microscopic structure of a fluid confined to a model slit pore for a number of thermodynamic states along a near-critical isochore of a homogeneous bulk fluid reservoir in equilibrium with the confined phase. To foster a quantitative discussion, it is convenient to distinguish between wall and core regions based upon the range of the fluid-wall interaction potential. The wall region is characterized by layering, that is, $\rho^{(1)}(z)$ is an oscillatory function of position with respect to the walls, indicating that the fluid is adsorbed by the walls. Layering is affected by both the relative strength of the fluid-wall interaction potential and its analytic form. In the core region the impact of the different form of the fluid-wall potential on details of the fluid's microscopic structure can be compensated for by adjusting f properly. If T is sufficiently larger than T_c of the homogeneous bulk reservoir, the core region appears to be homogeneous, too, i.e., $\rho_{\text{core}}^{(1)}(z) = \rho_c = \text{const}$. In the near-critical regime $T^* < 1.60$, however, the core region appears to be depleted with respect to the bulk reservoir, i.e., $\rho_{\text{core}}^{(1)}(z) < \rho_c$. This effect is more pronounced the closer T is to T_c.

From the density profiles $\rho^{(1)}(z)$ in Figs. 3 and 5, we are now in a position to give a microscopic rationale for

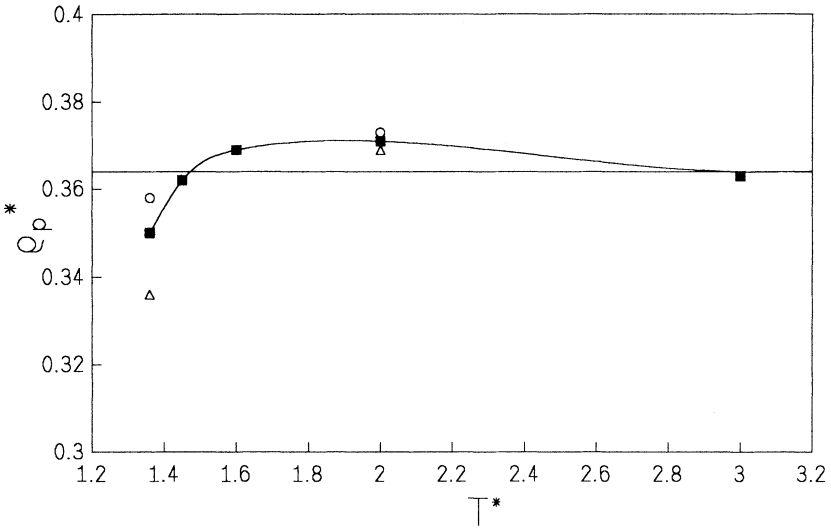

FIG. 11. The pore average density ρ_p^* as a function of temperature T^* for model A at $f=0.9836$ (■), model B at $f=0.86065$ (○), and $f=0.7377$ (△) obtained by numerical integration of $\rho^{(1)}(z)$. At $T^*=3.00$ the three data points fall on top of each other. Also shown is a cubic spline (——) to the results for model A to guide the eye. The solid horizontal line represents the constant density $\rho^*=0.365\cong\rho_c^*$ of the bulk reservoir.

the experimentally observed temperature dependence of the surface excess Γ along the critical isochore of the bulk reservoir. According to the microscopic definition

$$\Gamma(T)=\int_0^{s_z}[\rho^{(1)}(z;T)-\rho_c]dz=s_z[\rho_p(T)-\rho_c]\ , \qquad (17)$$

the temperature dependence of $\Gamma(T)$ along the (bulk) critical isochore is identical to that of the pore average density $\rho_p(T)$. In Fig. 11 $\rho_p(T)$ is plotted as a function of T for models A and B and three different values of f. At a sufficiently high temperature of $T^*=3.00$, $\rho_p(T)\cong 0.365\cong\rho_c^*$ regardless of f and the form of the fluid-wall interaction potential. As T is lowered, $\rho_p(T)$ increases until a maximum is reached. The increase is caused by stronger adsorption at the walls due to lower (average) kinetic energy of fluid molecules while the core region density remains constant at $\rho\cong\rho_c$ because T is still sufficiently higher than T_c to prevent depletion. However, as T is lowered further, $\rho_p(T)$ eventually decreases and reaches a value at $T^*=1.36\cong T_c$, which is significantly lower than ρ_c in all three cases displayed in Fig. 11. According to Figs. 3 and 5, this decline of $\rho_p(T)$ is a result of depletion in the core region which competes with a still increasing tendency of the walls to adsorb more fluid molecules. Therefore, depletion must not be viewed as drying at the walls. Since the volume of the core region exceeds by far the volume of the wall region at $s_z^*=20$, the "negative" contribution to $\rho_p(T)$ from the core region overwhelms the "positive" contribution from the wall region below a certain temperature threshold so that the net effect causes $\rho_p(T)$ from GCEMC to exhibit a temperature dependence strikingly similar to its experimental counterpart (see, for instance, Fig. 3 in [11]). We conclude that the experimentally observed decay of the surface excess Γ along the critical isochore as $T\rightarrow T_c+$ is caused by an increasing tendency to remove molecules predominantly from the core region. However, details of the effect depend crucially on an interplay between the relative strength of fluid-wall interactions and pore size.

The origin of depletion is elucidated by a gedanken experiment employing a homogeneous two-fluid van der Waals model for core region and bulk reservoir. On account of confinement of the fluids, compressibilities of core and bulk phases will eventually become different below some threshold temperature T_0 as $T\rightarrow T_c+$ along a near-critical isochore. Within the framework of the van der Waals equation of state, different compressibilities in two fluids maintained at the same ρ and T implies different critical points. In other words, at $T<T_0$ the core fluid is *effectively* different from the bulk fluid. A shift of the critical-point location inevitably affects the temperature and density dependence of the pressure in the core fluid. Hence, depletion is a phenomenon by which mechanical stability between core and bulk fluids is maintained at $T<T_0$. Besides confinement, a sufficiently close approach of the bulk critical point is indispensable in order for depletion to occur. Only if the bulk fluid is sufficiently critical does ξ reach a value comparable to the dimensions of the pore (i.e., s_z). From this point of view, depletion is a phenomenon driven by the criticality of the bulk fluid. The effect should, in principle, be independent of pore geometry and may be of significance whenever fluids in contact with mesoporous and colloidal materials approach their critical point.

ACKNOWLEDGMENTS

We are indebted to Professor Dr. Gerhard H. Findenegg (TU Berlin) for his persistent interest in this work and acknowledge in particular the many discussions we enjoyed that guided the direction of this work and helped us improve the presentation. M.S. thanks the Deutsche Forschungsgemeinschaft (DFG) for support and M.T. acknowledges support by the Deutsche Agentur für Raumfahrtangelegenheiten (DARA) under Grant No. 50 WM 9115. The authors are also grateful to the Scientific Council of Höchstleistungsrechenzentrum (HLRZ) at Forschungszentrum Jülich for a substantial allowance of computer time on the Cray Y-MP/864.

[1] R. J. Baxter, *Exactly Solved Models in Statistical Mechanics,* 2nd ed. (Academic, London, 1990).
[2] J. V. Sengers and J. M. H. Levelt Sengers, in *Progress in Liquid Physics,* edited by C. A. Croxton (Wiley, New York, 1978), pp. 103–174.
[3] D. Beysens, in *Proceedings of the VIIth European Symposium on Materials and Fluid Sciences in Microgravity, Oxford, 1990,* edited by B. Kaldeich (European Space Agency SP-295, Oxford, 1990), p. 355.
[4] S. Dietrich, in *Phase Transitions and Critical Phenomena,* edited by C. Domb and J. L. Lebowitz (Academic, London, 1988), Vol. 12.
[5] M. Schick, in *Liquides aux Interfaces,* Les Houches 1988 Session XLVIII, Course Nine, edited by J. Charvolin, J. Joanny, and J. Zinn-Justin (North-Holland, Amsterdam, 1990).
[6] M. E. Fisher and P. de Gennes, C. R. Acad. Sci. Ser. B **287**, 207 (1978).
[7] M. E. Fisher and H. J. Nakanishi, J. Chem. Phys. **75**, 5857 (1981).
[8] H. J. Nakanishi and M. E. Fisher, J. Chem. Phys. **78**, 3279 (1983).
[9] M. Thommes and G. H. Findenegg, Langmuir **10**, 4270 (1994).
[10] M. Thommes, G. H. Findenegg, and H. Lewandowski, Ber. Bunsenges. Phys. Chem. **98**, 477 (1994).
[11] M. Thommes, G. H. Findenegg, and M. Schoen, Langmuir **11**, 2137 (1994).
[12] M. Schoen, *Computer Simulation of Condensed Phases in Complex Geometries* (Springer-Verlag, Heidelberg, 1993).
[13] M. P. Allen and D. J. Tildesley, *Computer Simulation of Liquids* (Clarendon, Oxford, 1987).
[14] M. Schoen, J. Comput. Phys. **118**, 159 (1995).
[15] E. J. Bottani and V. A. Bakaev, Langmuir **10**, 1550 (1994).
[16] W. van Megen and I. K. Snook, Mol. Phys. **45**, 629 (1982).
[17] J. R. Recht and A. Z. Panagiotopoulos, Mol. Phys. **80**, 843 (1993).
[18] K. K. Mon and K. Binder, J. Chem. Phys. **96**, 6989 (1992).
[19] J. P. Hansen and L. Verlet, Phys. Rev. **184**, 151 (1969).
[20] J. P. Hansen and I. R. McDonald, *Theory of Simple Liquids,* 2nd ed. (Academic, London, 1986).
[21] F. Vesely, *Computerexperimente an Flüssigkeitsmodellen* (Physik-Verlag, Weinheim, 1978).
[22] J. A. Barker and D. Henderson, Annu. Rev. Phys. Chem. **23**, 439 (1972).
[23] L. Verlet, Phys. Rev. **159**, 98 (1967).
[24] D. J. Adams, Mol. Phys. **37**, 211 (1975).
[25] M. Plischke and B. Bergersen, *Equilibrium Statistical Physics,* 2nd ed. (World Scientific, Singapore, 1994).
[26] M. Schoen, D. J. Diestler, and J. H. Cushman, J. Chem. Phys. **87**, 5464 (1987).
[27] M. Schoen, D. J. Diestler, and J. H. Cushman, J. Chem. Phys. **101**, 6865 (1994).
[28] W. van Megen and I. K. Snook, Mol. Phys. **54**, 741 (1985).
[29] P. B. Balbuena and K. E. Gubbins, Langmuir **9**, 1801 (1993).
[30] C. Lastoskie, K. E. Gubbins, and N. Quirke, Langmuir **9**, 2693 (1993).
[31] U. Marini Bettolo Marconi, Phys. Rev. A **38**, 6267 (1988).
[32] A. Jamnik and D. Bratko, Chem. Phys. Lett. **203**, 465 (1993).
[33] M. Schoen and M. Thommes (unpublished); M. Thommes, M. Schoen, and G. H. Findenegg, in *Physical Sciences in Microgravity,* Vol. 464 of Lecture Notes in Physics, edited by B. Feuerbacher and L. Ratke (Springer-Verlag, Heidelberg, 1995).